





Crystal growth, transport, and magnetic properties of quasi-one-dimensional La_3MnBi_5

Cuiwei Zhang ^{1,2} Yaxian Wang ^{1,*} Jiaxin Zheng,^{1,5} Liang Du ^{1,5} Yong Li,¹ Xin Han,^{1,2} Enke Liu ^{1,3}
Quansheng Wu,^{1,3,†} and Youguo Shi^{1,2,4,‡}

¹Beijing National Laboratory for Condensed Matter Physics and Institute of Physics, Chinese Academy of Sciences, Beijing 100190, China

²Center of Materials Science and Optoelectronics Engineering, University of Chinese Academy of Sciences, Beijing 100190, China

³School of Physical Sciences, University of Chinese Academy of Sciences, Beijing 100190, China

⁴Songshan Lake Materials Laboratory, Dongguan, Guangdong 523808, China

⁵College of Physics and Technology, Guangxi Normal University, Guilin, Guangxi 541004, China



(Received 24 September 2023; accepted 6 February 2024; published 13 March 2024)

Quasi-one-dimensional (Q1D) materials featuring chainlike structures with half-filled transition metal d shells offer a unique playground to study emergent spin order and quasiparticle interactions. In this paper, we successfully grow and comprehensively analyze a manganese-based compound, La_3MnBi_5 , characterized by face-sharing MnBi_6 spin chains. At low temperatures, La_3MnBi_5 adopts an antiferromagnetic spin configuration and exhibits various anomalies in both magnetization and specific heat measurements, signatures for successive magnetic phase transitions upon varying temperature. The electrical transport reveals its metallic behavior, likely contributed by the itinerant La electrons. We reveal complex hysteretic behaviors in its magnetoresistance under different transport configurations, indicating the interplay between the interchain and intrachain coupling in this Q1D material. In this paper, we offer insights into the understanding of the unique magnetic and electronic properties of the R_3MX_5 family, and we hope to spark further investigation into the precise magnetic structure and spin physics in similar systems.

DOI: [10.1103/PhysRevMaterials.8.034402](https://doi.org/10.1103/PhysRevMaterials.8.034402)

I. INTRODUCTION

Quasi-one-dimensional (Q1D) materials consisting of one-dimensional (1D) atomic chain or columnlike motifs have exotic properties arising from their low-dimensional structures and thus serve as a unique platform for exploring emerging physical phenomena, such as charge density waves [1–4], Luttinger liquid phases [5–7], spin-Peierls transitions [8–10], and superconductivity [11–15]. Specifically, 1D spin chains, in coexistence with interchain coupling in low-dimensional materials, offer a playground to study various model magnetism, including but not limited to the Ising model [16], Heisenberg model [17], and even the XY -type model [18]. Although the Mermin-Wagner theorem indicates that an ideal 1D spin chain can host no long-range magnetic order at finite temperature due to strong thermal fluctuations [19], the interchain interaction can play a key role in forming and stabilizing the long-range magnetic order in Q1D systems, though it is much weaker than the intrachain interaction [20]. For example, La_3MnAs_5 has a spin chain of MnAs_6 and features a ferromagnetic (FM) phase transition at 112 K, and it is indicated that the itinerant electrons from La atom contribute to orbital hybridization and mediate interchain interaction between the 1D MnAs_6 spin chains [21]. Its sister compound La_3CrAs_5 also shows a FM phase transition at 50 K with a weak interchain interaction between the CrAs_6 spin

chains [22]. Furthermore, Q1D iron selenide $\text{Ba}_9\text{Fe}_3\text{Se}_{15}$ undergoes a FM transition at 14 K [23], while no long-range magnetic order, but a spin-glass transition has been observed in $\text{Ba}_9\text{Co}_3\text{Se}_{15}$ [24]. These studies indicate that the R_3MX_5 (R = lanthanide or alkali earth metal; M = transition metal; X = chalcogen or pnictogen) materials harbor rich spin configurations with great opportunities to study 1D spin-chainlike magnetism in bulk materials [21–29].

Among the Q1D materials, the manganese-based compounds have attracted considerable attention owing to their unique crystalline structure consisting of $[\text{Mn}_6\text{Bi}_5]^-$ chains [13–15,30]. Recently, the Q1D antiferromagnetic (AFM) material KMn_6Bi_5 has been successfully synthesized, and emerging superconductivity is observed as its AFM transition is suppressed at the pressure of 13 GPa [13]. Afterwards, members of its isostructural compounds RbMn_6Bi_5 and CsMn_6Bi_5 crystals were synthesized and shown to host pressure-induced superconductivity on the border of AFM order in the phase diagrams [14,15]. However, for another isostructural compound NaMn_6Bi_5 , which is found to have lower AFM transition temperature, the critical pressure to induce superconductivity is expected to be less as well, yet no bulk superconductivity is observed under the measured pressure even up to 69 GPa [30]. These studies highlight the complexity in the magnetic order and its interplay with other degrees of freedom in these Q1D manganese-based materials. However, although single crystals Ln_3MnBi_5 ($\text{Ln} = \text{La} - \text{Nd}$) have been synthesized, a comprehensive understanding of their magnetic properties remains elusive [31].

Herein, we report on the synthesis, structure, and magnetic and transport properties of La_3MnBi_5 , a member of the

*yaxianw@iphy.ac.cn

†quansheng.wu@iphy.ac.cn

‡ygshi@iphy.ac.cn

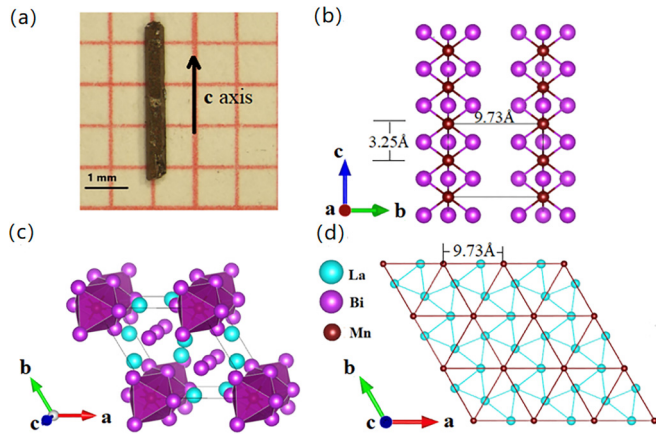


FIG. 1. (a) An image of a millimeter-sized single crystal of La_3MnBi_5 . The rod direction is along the crystallographic c axis. (b) The crystal structure of La_3MnBi_5 viewed along the a axis, with unit cell outlined by the black box. (c) The crystal structure of La_3MnBi_5 viewed along the c axis, highlighting the quasi-one-dimensional (Q1D) chain-forming MnBi_6 octahedra. (d) The triangular lattice formed by Mn atoms is shown in red, and the blue lines and dots indicate the La network.

R_3MX_5 family consisting of 1D MnBi_6 spin chains. We find that bulk La_3MnBi_5 prefers an AFM spin configuration at low temperature and exhibits anomalies when raising temperature or applying external fields. We analyze these features in magnetization and specific heat measurements, which we believe to be a strong indication of successive magnetic phase transitions. Further, electrical transport measurements reveal its metallic behavior, possibly arising from the itinerant La electrons, and meanwhile, the magnetoresistance (MR) data show a clear correlation with its magnetic properties. While further studies are needed to pinpoint the magnetic structure associated with each phase, our work underscores the complex spin physics resulting from interchain and intrachain coupling, the understanding of which is the fundamentals of probing and manipulating spins in Q1D materials.

II. EXPERIMENTAL METHODS

A. Growth

Single crystals of La_3MnBi_5 were synthesized using the flux method. The starting materials La (ingot, 99.9%), Mn (piece, 99.99%), and Bi (lump, 99.999%) were mixed in an Ar-filled glove box at a molar ratio of La:Mn:Bi = 1:6:9. The mixture was placed in an alumina crucible and sealed in an evacuated quartz tube. The tube was heated to 900 °C for 10 h and dwelt for 20 h. Then the tube was slowly cooled to 700 °C at a rate of 2 °C/h, followed by separation of the crystals from the flux by centrifugation. Rodlike crystals were obtained as shown in Fig. 1(a), which is along the c axis of the crystal.

B. Characterization

The crystal structure of the as-grown crystals were identified via single-crystal x-ray diffraction (XRD) measurements conducted on a Bruker D8 VENTURE diffractometer using Mo $K\alpha$ radiation ($\lambda = 0.71073 \text{ \AA}$). Structure solutions

were obtained by intrinsic phasing methods using the program APEX3, and the crystalline structure was refined by the full-matrix least square method on F^2 using the SHELXL-2018/3 program [32,33]. Elemental analysis of the crystals was performed using energy dispersive x-ray spectroscopy in a Hitachi S-4800 scanning electron microscopy at an accelerating voltage of 15 kV.

C. Transport

The magnetic properties of La_3MnBi_5 crystals were obtained using a magnetic properties measurement system (Quantum Design Inc.) and a physical property measurement system (PPMS-16 T, Quantum Design Inc.). Magnetic susceptibility was measured under different applied magnetic fields in field-cooling (FC) and zero-field-cooling (ZFC) modes. Isothermal magnetization was measured at several fixed temperatures by sweeping the applied field from -16 to 16 T. The specific heat was measured by a thermal relaxation method using a PPMS-9 T. Electrical resistivity (ρ) and MR were measured in the PPMS-16 T with the standard four-probe method from 2 to 300 K. All these measurements were performed with the c axis of the single crystal both parallel and perpendicular to the external magnetic field.

III. RESULTS AND DISCUSSIONS

A. Crystal structure

La_3MnBi_5 crystallizes into rodlike morphologies having length and radius of ~ 3 and ~ 0.2 mm, respectively [Fig. 1(a)]. The single-crystal XRD measurement reveals that La_3MnBi_5 exhibits the anti- $\text{Hf}_5\text{Sn}_3\text{Cu}$ structure type with space group $P6_3/mcm$ (No.193), which is consistent with the previous single-crystalline study [31]. It has an a lattice parameter of 9.73 \AA and a c lattice parameter of 6.50 \AA [Figs. 1(b) and 1(d)]. The sketches of the crystal structure of La_3MnBi_5 are summarized in Fig. 1, and more detailed crystallographic data and crystalline parameters obtained from the single-crystal XRD measurements are summarized in Tables S1 and S2 in the Supplemental Material (SM) [34]. As shown in Fig. 1(c), the crystal structure of La_3MnBi_5 consists of two 1D parts along the c axis: face-sharing MnBi_6 octahedra and the chain-forming Bi atoms. These octahedral MnBi_6 and Bi chains are separated by the La ions. Figure 1(b) shows the side view of the internal structure of the MnBi_6 octahedra chains, the distance between which is 9.73 \AA , significantly larger than that adjacent Mn ions within the chain. Thus, the crystal structure of La_3MnBi_5 shows a strong 1D character. In addition, Fig. 1(d) shows the trigonal arrangement of the MnBi_6 octahedra in the ab plane. The Q1D and meanwhile trigonal arrangement of Mn ions make it appealing to study the magnetic order of this material.

B. Magnetism

Temperature-dependent magnetization $M(T)$ data measured at $\mu_0 H = 1 \text{ T}$ ($H \perp c$) are presented in the inset of Fig. 2(a). The $M(T)$ curve shows a hump $\sim 45 \text{ K}$ and a sudden drop at 24 K . These transitions can be seen more clearly from the corresponding first-order derivative of $M(T)$. Within

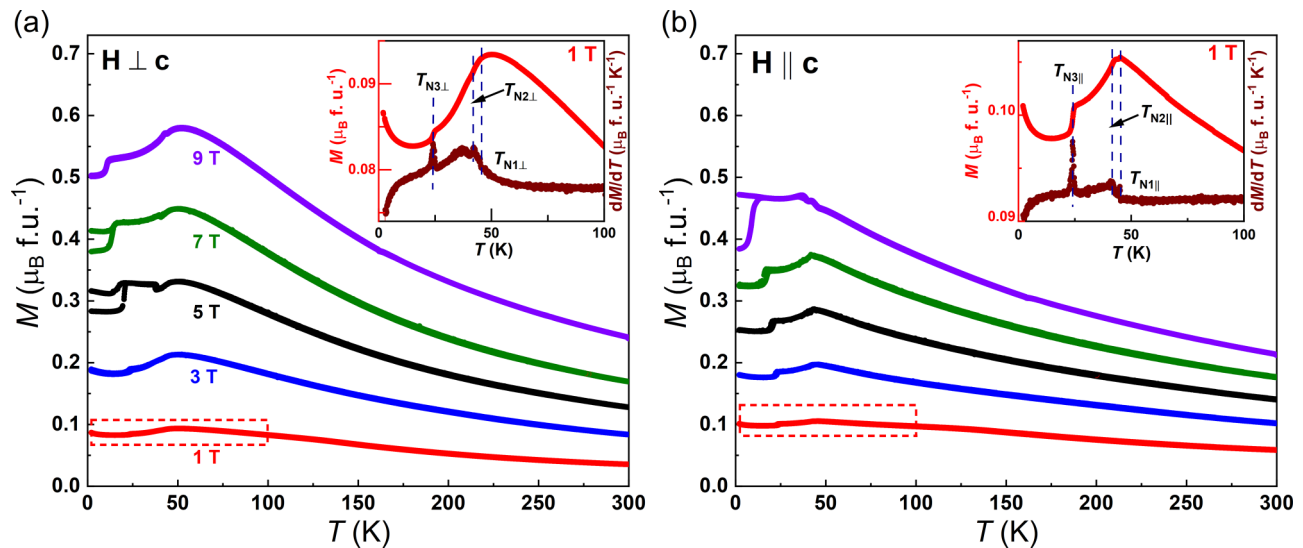


FIG. 2. Temperature-dependent magnetization of La_3MnBi_5 measured under (a) $H \perp c$ and (b) $H \parallel c$. Insets of (a) and (b) show the low-field magnetization and their corresponding first derivatives measured at $\mu_0 H = 1$ T.

the measured temperature range, there are three anomalies in $M(T)$, marked as $T_{N1\perp}$ (45 K), $T_{N2\perp}$ (42 K), and $T_{N3\perp}$ (24 K), an indication of successive magnetic transitions in La_3MnBi_5 . The subscript $\perp(\parallel)$ stands for $H \perp c$ ($H \parallel c$) in this section. Meanwhile, $M(T)$ measured under varied H for $H \perp c$ are shown in Fig. 2(a). With increasing magnetic field, the transitions at $T_{N1\perp}$ and $T_{N2\perp}$ have no obvious change, while the sudden drop at $T_{N3\perp}$ moved to lower temperature, indicating AFM ordering at $T_{N3\perp}$ (for more details of dM/dT curves, see Fig. S1(a) in the SM [34]). In addition, the ZFC and FC curves measured under 5 and 7 T show divergence at low temperature but overlap under 9 T, consistent with $M(H)$ data, which will be discussed as follows.

For $H \parallel c$, $M(T)$ curves presented in Fig. 2(b) show similar behavior to those for $H \perp c$, with anomalous temperature dependence at 45 K ($T_{N1\parallel}$), 42 K ($T_{N2\parallel}$), and 24 K ($T_{N3\parallel}$). As the magnetic field increases, the transition at $T_{N2\parallel}$ slightly moves to lower temperature, meanwhile $T_{N1\parallel}$ stays almost unchanged and $T_{N3\parallel}$ clearly decreases with external field, the latter of which is like that for $H \perp c$ (for more details of dM/dT curves, see Fig. S1(b) in the SM [34]).

We then fit χ^{-1} vs T for the $\chi^{-1}(T)$ data measured at $\mu_0 H = 1$ T by the Curie-Weiss formula $\chi = C/(T - T_\theta)$, where C is the Curie constant and T_θ is the Weiss temperature (Fig. S2 in the SM [34]). The obtained T_θ values and calculated effective moment for the two field directions under varying H fields are summarized in Table S3 in the SM [34]. The negative values of T_θ for both $H \perp c$ and $H \parallel c$ indicate AFM interaction between magnetic moments of Mn ions. The large T_θ values for $H \parallel c$ suggest the strong magnetic interaction along the c axis, i.e., the spin chain direction. Typically, the effective moment can be estimated by the Curie constant $\mu_{\text{eff}} = \sqrt{8C} \mu_B$. We find the effective moment for $H \parallel c$ to be $6.92 \mu_B$ under $\mu_0 H = 7$ T, larger than the theoretical value of Mn^{2+} ion in its high spin state. For $H \perp c$, the effective moment μ_{eff} is close to the theoretical value under $\mu_0 H = 3$ T and above. Furthermore, considering the 1D structure of La_3MnBi_5 , we have attempted to fit the

magnetic susceptibility data using 1D magnetism models proposed by Wagner and Friedberg [35] and Emori *et al.* [36]. We found that both models work well at high temperature but show strong deviation below ~ 120 K (Fig. S3 in the SM [34]). This might be because, although the La_3MnBi_5 lattice features 1D-like MnBi_6 spin chains, the magnetic properties do not fully obey strong 1D behavior due to the interchain coupling and the itinerant electrons. Taken together, possible reasons for the deviation of the effective moment from the theoretical value may include FM impurities (though not large enough) as well as single-ion anisotropy [39–41], yet further studies are needed to determine the magnetic configuration.

To better investigate the possible magnetic transitions in La_3MnBi_5 , we carry out temperature-dependent specific heat (C_p) measurements with and without an external field. In the absence of external field, the $C_p(T)$ curve shows two anomalies, seen by a λ -shaped curve with a peak at T_{N1} and a hump at T_{N2} [Fig. 3(a)]. When plotting the temperature dependence of the specific heat and magnetization as well as its derivative (Fig. S4 in the SM [34]), we find the anomalies in $C_p(T)$ appear at the same temperatures in the $M(T)$ curve and its derivative. Since we have measured the crystal structure at 30 K and did not observe a structural change (see Table S1 in the SM [34]), these highly indicate that long-range magnetic transitions occur at T_{N1} and T_{N2} . Moreover, we have measured $C_p(T)$ under different magnetic fields for $H \parallel c$. A clear shift of T_{N2} to lower temperature is seen with increasing magnetic field (Fig. S4(d) in the SM [34]), consistent with magnetization measurements discussed earlier. We further study the magnetic contribution to the entropy of La_3MnBi_5 by subtracting the C_p data of its nonmagnetic analog La_3MgBi_5 (mass corrected), shown in Fig. 3(b). The $C_{\text{mag}}(T)$ curve shows a peak ~ 45 K corresponding to the magnetic transition. The magnetic entropy S_{mag} approaches saturation at 150 K with a value of $15.9 \text{ J mol}^{-1} \text{ K}^{-1}$, very close to the theoretical limit for the high spin state of Mn^{2+} , i.e., $S_{\text{mag}} = R \ln(2J + 1)$ [blue curve in Fig. 3(b)]. The magnetic entropy at T_{N1} reaches

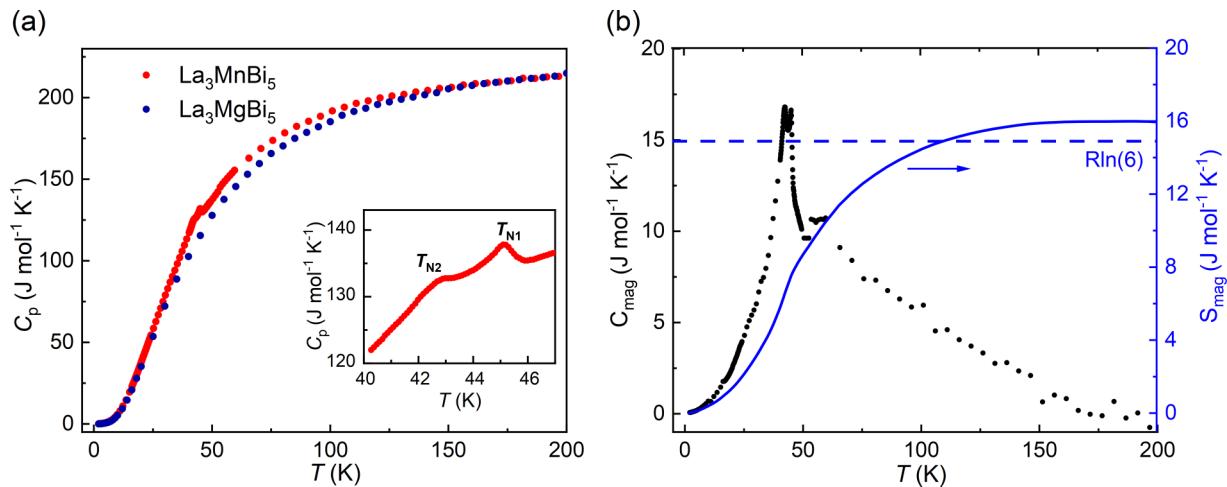


FIG. 3. (a) Temperature-dependent specific heat for La_3MnBi_5 and its nonmagnetic counterpart La_3MgBi_5 . Inset shows the enlarged region near the possible magnetic transition. (b) Left: Temperature-dependent magnetic specific heat C_{mag} . Right: The magnetic entropy S_{mag} as a function of temperature < 200 K.

46% of the saturation value, indicating the entropy gain above $T_{\text{N}1}$ is likely due to the formation of short-range spin orders of Mn [42]. Moreover, there is no obvious anomaly at $T_{\text{N}3}$, possibly because the magnetic entropy has been released completely above $T_{\text{N}3}$; similar phenomena have been observed in other $R_3\text{MX}_5$ compounds [43].

The long-range AFM order is likely to arise from Mn-Mn interchain interaction, although the Mn-Mn interchain distance of 9.73 Å is much larger than their intrachain distance of 3.25 Å; thus, interaction is expected to be smaller. A recent study on an isoelectronic compound La_3MnAs_5 revealed a FM transition at 112 K, and density functional theory calculations show the orbital hybridization between the MnAs_6 chain and the La atom around the Fermi level, suggesting interchain spin coupling via itinerant electrons from La [21], i.e., a RKKY interaction. La_3MnBi_5 could have the similar magnetism mechanism with La_3MnAs_5 due to their nearly identical electronic configurations. However, La_3MnBi_5 features AFM ordering with a lower magnetic transition temperature than that of La_3MnAs_5 . We note that the distance of interchain is 9.73 and 8.99 Å for La_3MnBi_5 and La_3MnAs_5 , respectively. Therefore, increasing of the interchain distance may cause the interchain interaction to become weaker, and thus, the long-range magnetic order forms at lower temperature. Furthermore, for the RKKY interaction, local spins can couple ferromagnetically or antiferromagnetically depending on the electronic DOS near the Fermi level and the distance of local spins [44]. These factors can contribute to the complex magnetic ordering in La_3MnBi_5 , but a more comprehensive theoretical study is needed to clarify the origin.

Isothermal magnetization $M(H)$ data measured with $H \perp c$ at 5 and 20 K are presented in Fig. 4(a). At 5 K, a hysteretic transition occurs in field-sweep up and down measurements, consistent with our observation that $M(T)$ data in which the ZFC and FC curves measured under $\mu_0 H = 5$ and 7 T show divergence [Fig. 2(a)]. The critical fields in field-sweep up and down measurements are marked as H_{up} and H_{down} . At higher temperature of 20 K, both H_{up} and H_{down} move to lower field

and the difference between them decreases accompanying a shrinking range of hysteresis. For $H \parallel c$, $M(H)$ is measured at four different temperatures, shown in Fig. 4(b). In this case, the range of hysteresis decreases with H_{up} and H_{down} moving to higher field at higher temperatures. The hysteretic transition remains visible below $T_{\text{N}2}$ but disappears above it for both $H \perp c$ and $H \parallel c$ (for data at 50 K, see Figs. S5(c) and S5(d) in the SM [34]), indicating the field-induced hysteretic transition is related to the anomaly at $T_{\text{N}3}$. The hysteresis loop is an indication for a possible first-order transition with an existing crossover between the two magnetic phases. Such a hysteretic transition has also been discovered in $\text{PbCuSO}_4(\text{OH})_2$, where the spin chains formed by Cu^{2+} ions transit from the ground state of a helix arrangement to an excited magnetic phase likely through a first-order transition [45]. The linear behavior and nonsaturation of the $M(H)$ curves at high fields further confirm the AFM coupling. In addition, for $H \perp c$ and $H \parallel c$, we see a nonlinear dependence of $M(H)$ at below 1 T. We thus perform room-temperature measurements and observe a small hysteresis at ~ 0 T (Fig. S5 in the SM [34]). Further, an obvious divergence of ZFC and FC curves shows up < 100 K under $\mu_0 H = 0.1$ T (see Figs. S5(a) and S5(b) in the SM [34]). These together hint of a MnBi FM impurity-related effect which is likely to induce the nonlinear behavior in the $M(H)$ curve [46].

C. Electrical transport

Electrical transport measurements with various configurations of the applied current (I) and magnetic field (H) were carried out from 2 K to room temperature, shown in Figs. 5(a), 5(c), and 5(e). The subscript \parallel (\perp) stands for $I \parallel c$ ($I \perp c$) in this section. First, $\rho_{\parallel}(T)$ measured with the applied magnetic field perpendicular to the c axis is presented in Fig. 5(a). Within the measured temperature range, the resistivity of La_3MnBi_5 increases with temperature, showing a metallic behavior. The $\rho_{\parallel}(T)$ curve shows an anomaly at 45 K consistent with the transition at $T_{\text{N}1}$ observed in the $M(T)$ curves. The MR, following the formula $\frac{\rho(H) - \rho(0)}{\rho(0)}$, is

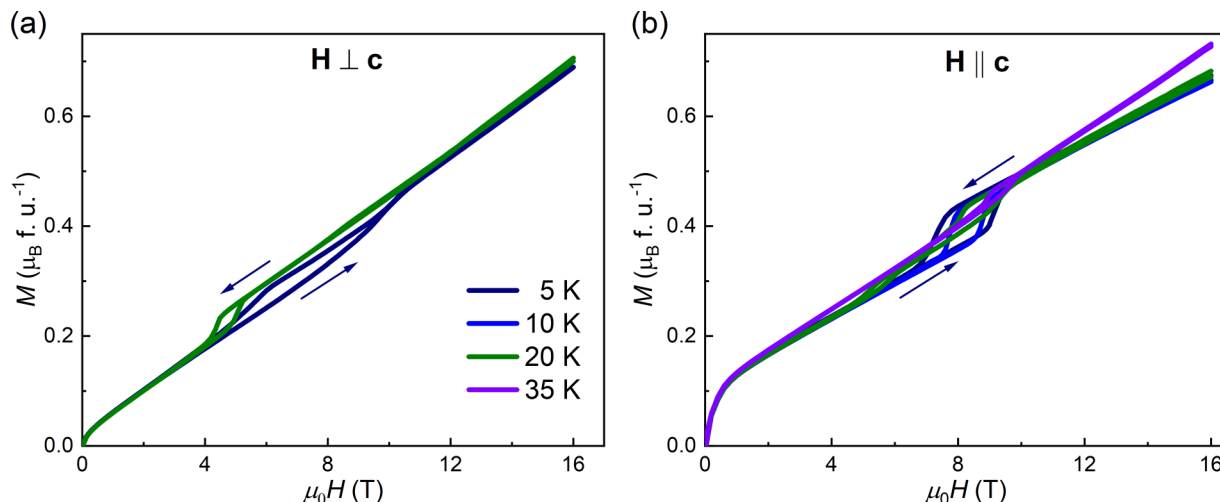


FIG. 4. Isothermal magnetizations of La_3MnBi_5 measured with (a) $H \perp c$ and (b) $H \parallel c$. The arrows refer to the field-sweeping direction.

−13% at 2 K under a magnetic field of 9 T. Here, $\rho_{\parallel}(T)$ measured with $H \parallel c$ shows nearly identical behavior with that for $H \perp c$ shown in Fig. 5(c). However, when applying current perpendicular to the c axis, the resistivity of La_3MnBi_5 drops with increasing temperature at above 45 K [Fig. 5(e)]. Further, the resistivity is ~ 5 times of that for ρ_{\parallel} , indicating a strongly anisotropic behavior. The transition temperature at 45 K for $\rho_{\perp}(T)$ coincides with that of the $\rho_{\parallel}(T)$ curve, likely caused by suppressed magnetic scattering as the magnetic order forms. Different from negative MR for $I \parallel c$, in this case the MR is 18% at 2 K under a magnetic field of 9 T. The strong anisotropy originates from its Q1D structure and the negative

(positive) MR for $I \parallel c$ ($I \perp c$) suggest that the intrachain spin arrangement is probably different from interchain spin arrangement.

Field-dependent MR data measured at different temperatures are presented in Figs. 5(b), 5(d), and 5(f), with the same directions of the current and magnetic field illustrated in insets of Figs. 5(a), 5(c), and 5(e). Here, MR_{\parallel} measured with $H \perp c$ is presented in Fig. 5(b). At 2 K, with increasing field, MR_{\parallel} increases first then suddenly decreases accompanying a sign changing from positive to negative as well as a hysteretic transition occurring in field-sweep up and down measurements. With increasing temperature, the

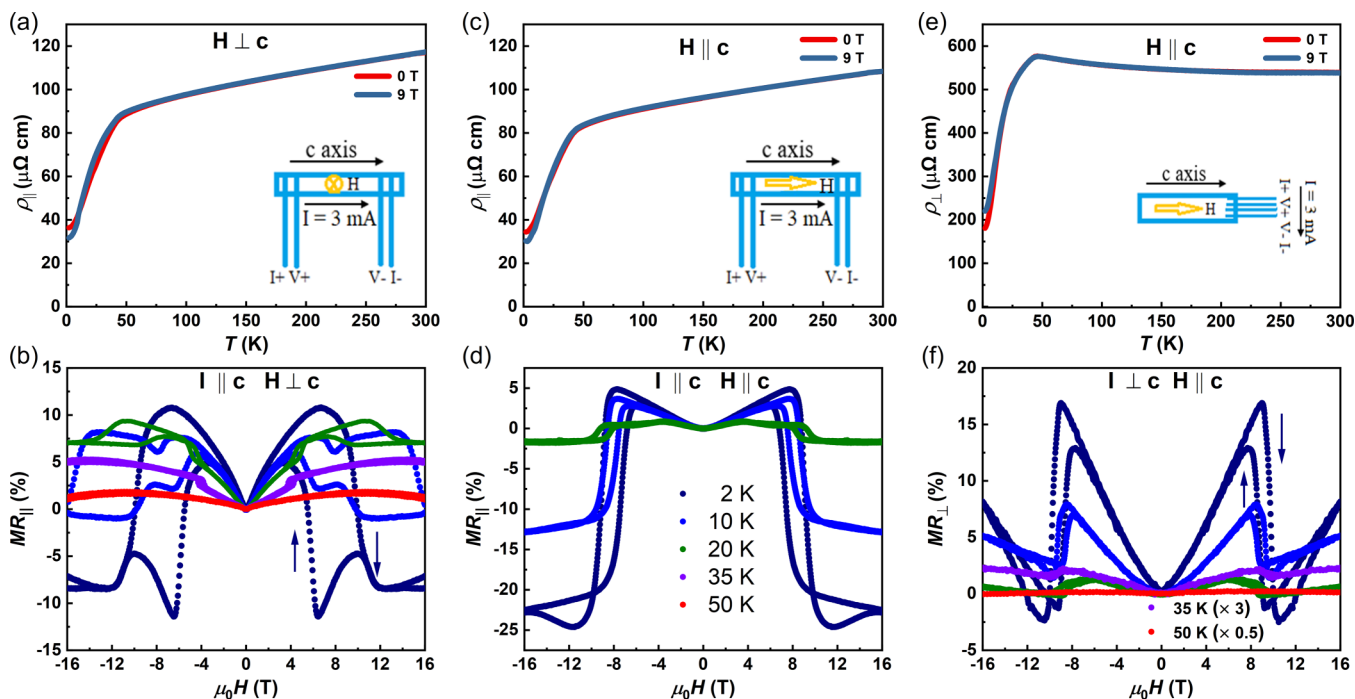


FIG. 5. (a), (c), and (e) Temperature-dependent resistivity of La_3MnBi_5 measured under zero and 9 T magnetic field. The insets show the different configurations of the applied current and magnetic field in the measurements. (b), (d), and (f) The corresponding field-dependent magnetoresistance (MR) of La_3MnBi_5 measured under varying temperatures.

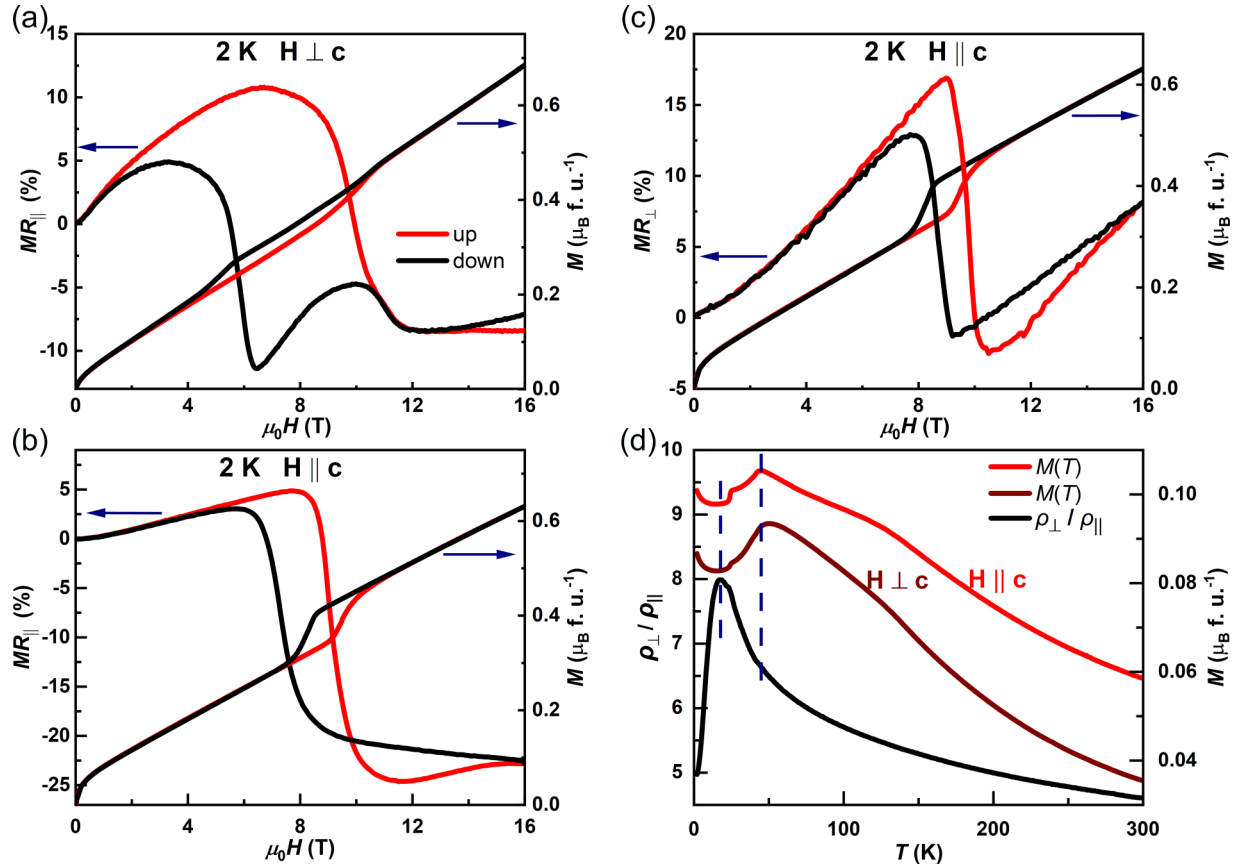


FIG. 6. (a)–(c) Field-dependent magnetoresistance (MR) and magnetization of La_3MnBi_5 at 2 K, with MR data consistent with those in Fig. 5. Up and down arrows refer to the field-sweeping directions. (d) Resistivity anisotropy and magnetization of La_3MnBi_5 measured at different temperatures with $H \perp c$ and $H \parallel c$ under $\mu_0 H = 1$ T.

range of hysteresis decreases and MR_{\parallel} becomes positive at >10 K. The hysteretic transition disappears at $T > T_{N2}$ and the value of MR_{\parallel} becomes close to zero. More specifically, there are two field-induced hysteretic transitions in MR_{\parallel} at $T < T_{N3}$. Here, MR_{\parallel} measured with $H \parallel c$ shows a similar behavior to that for $H \perp c$ presented in Fig. 5(d), while it has only one hysteretic transition at $T < T_{N3}$. Also, MR_{\perp} curves measured with $H \parallel c$ presented in Fig. 5(f) keep the hysteretic transition, but it is mostly positive within the measured temperature.

To better reveal the correlation between the magnetic properties and electrical transport properties of La_3MnBi_5 , we plot the field-dependent MR and magnetization at 2 K in Fig. 6. For $H \perp c$, though MR and $M(H)$ show a similar hysteretic manner, the MR has more complex behavior than $M(H)$ at high field since the exact alignment of in-plane field with respect to the crystallographic axis is difficult to determine under this configuration [Fig. 6(a)]. For $H \parallel c$, MR correlates well with $M(H)$, shown in Figs. 6(b)–6(c). Finally, the anisotropy in electrical resistivity under $\mu_0 H = 1$ T is presented in Fig. 6(d). As temperature decreases from room temperature, the resistivity anisotropy first increases, showing a kink at T_{N1} and starts to decrease below $T < T_{N3}$, denoted by the blue dashed lines. The two temperatures agree with the successive transition features in $M(T)$ curves, indicating that the electrical transport properties are strongly coupled with magnetic properties.

The MR is theoretically predicted to be positive for an AFM metal with the magnetic field applied along the easy axis, while in the FM and paramagnetic case, the MR is usually negative [47]. The behavior that MR_{\parallel} changes from positive to negative is thus likely due to the change of magnetic configurations. Specifically, in the spin-alignment scenario, MR is dominated by spin scattering, i.e., the interaction between the itinerant spins and the lattice spins. AFM coupling usually generates stronger spin disorder scattering than FM coupling, resulting in a positive MR. With the magnetic field increasing, spin-disorder scattering will decrease as the spins are gradually polarized to the field direction, resulting in negative MR. For example, under high magnetic field, there can be a field-induced magnetic transition to a canted-AFM phase having an FM component, thus causing negative MR. The field-induced hysteretic transition in both $M(H)$ and MR implies a first-order magnetic phase transition, which has been observed in $\text{Ce}(\text{Fe}_{0.92}\text{Al}_{0.04})_2$ featuring hysteretic transport correlated with a FM-to-AFM first-order phase transition [48].

IV. CONCLUSIONS

In summary, we have successfully grown millimeter-scale single crystals of Q1D La_3MnBi_5 featuring MnBi_6 octahedra chains. We systematically studied its magnetization, specific heat, and electrical transport at various temperatures and

applied external fields. We observed multiple anomalies at <50 K, indicating complex magnetic phase transitions in La_3MnBi_5 that arise from the coexistence of the interchain and intrachain interactions. In addition, high magnetic field can induce a transition characterized by a hysteresis behavior in both magnetization and MR upon varying the field, which clearly shows correlation between the transport and the magnetic configuration. Further, we show a strong anisotropy in its electrical transport due to its Q1D structure. In this paper, we show the complex magnetic properties arising from the intertwined Q1D spin-chain structure and 3D electronic structure and highlight the interplay between the electron and spin degrees of freedom. While the precise magnetic structure in each phase needs further neutron diffraction or theoretical insights, the Ln_3MnBi_5 family offers a platform

to study various of magnetic phase transition mechanisms in low-dimensional materials.

ACKNOWLEDGMENTS

This paper is supported by the National Natural Science Foundation of China (Grants No. U22A6005, No. U2032204, and No. 12274436), the Chinese Academy of Sciences (Grants No. YSBR047 and No. E2K5071), the Strategic Priority Research Program of the Chinese Academy of Sciences (Grant No. XDB33010000), the Informatization Plan of Chinese Academy of Sciences (Grant No. CAS-WX2021SF-0102), the Center for Materials Genome, and the Synergetic Extreme Condition User Facility (SECUF).

-
- [1] G. Grüner, The dynamics of charge-density waves, *Rev. Mod. Phys.* **60**, 1129 (1988).
- [2] F. W. Boswell, A. Prodan, and J. K. Brandon, Charge-density waves in the quasi-one-dimensional compounds NbTe_4 and TaTe_4 , *J. Phys. C: Solid State Phys.* **16**, 1067 (1983).
- [3] S. J. Denholme, A. Yukawa, K. Tsumura, M. Nagao, R. Tamura, S. Watauchi, I. Tanaka, H. Takayanagi, and N. Miyakawa, Coexistence of superconductivity and charge-density wave in the quasi-one-dimensional material HfTe_3 , *Sci. Rep.* **7**, 45217 (2017).
- [4] J. Gooth, B. Bradlyn, S. Honnali, C. Schindler, N. Kumar, J. Noky, Y. Qi, C. Shekhar, Y. Sun, Z. Wang *et al.*, Axionic charge-density wave in the Weyl semimetal $(\text{TaSe}_4)_2\text{I}$, *Nature (London)* **575**, 315 (2019).
- [5] J. Voit, One-dimensional Fermi liquids, *Rep. Prog. Phys.* **58**, 977 (1995).
- [6] M. Nakamura, A. Sekiyama, H. Namatame, A. Fujimori, H. Yoshihara, T. Ohtani, A. Misu, and M. Takano, Metal-semiconductor transition and Luttinger-liquid behavior in quasi-one-dimensional BaVS_3 studied by photoemission spectroscopy, *Phys. Rev. B* **49**, 16191 (1994).
- [7] Q. Faure, S. Takayoshi, V. Simonet, B. Grenier, M. Månsson, J. S. White, G. S. Tucker, C. Rüegg, P. Lejay, T. Giamarchi *et al.*, Tomonaga-Luttinger liquid spin dynamics in the quasi-one-dimensional Ising-like antiferromagnet $\text{BaCo}_2\text{V}_2\text{O}_8$, *Phys. Rev. Lett.* **123**, 027204 (2019).
- [8] A. I. Buzdin and L. N. Bulaevskii, Spin-Peierls transition in quasi-one-dimensional crystals, *Sov. Phys. Usp.* **23**, 409 (1980).
- [9] M. Hase, I. Terasaki, and K. Uchinokura, Observation of the spin-Peierls transition in linear Cu^{2+} (spin $-\frac{1}{2}$) chains in an inorganic compound CuGeO_3 , *Phys. Rev. Lett.* **70**, 3651 (1993).
- [10] J. M. Law, C. Hoch, R. Glaum, I. Heinmaa, R. Stern, J. Kang, C. Lee, M.-H. Whangbo, and R. K. Kremer, Spin-Peierls transition in the $S = \frac{1}{2}$ compound TiPO_4 featuring large intrachain coupling, *Phys. Rev. B* **83**, 180414(R) (2011).
- [11] J.-K. Bao, J.-Y. Liu, C.-W. Ma, Z.-H. Meng, Z.-T. Tang, Y.-L. Sun, H.-F. Zhai, H. Jiang, H. Bai, C.-M. Feng *et al.*, Superconductivity in quasi-one-dimensional $\text{K}_2\text{Cr}_3\text{As}_3$ with significant electron correlations, *Phys. Rev. X* **5**, 011013 (2015).
- [12] H. Takahashi, A. Sugimoto, Y. Nambu, T. Yamauchi, Y. Hirata, T. Kawakami, M. Avdeev, K. Matsubayashi, F. Du, C. Kawashima *et al.*, Pressure-induced superconductivity in the iron-based ladder material BaFe_2S_3 , *Nat. Mater.* **14**, 1008 (2015).
- [13] Z. Y. Liu, Q. X. Dong, P. T. Yang, P. F. Shan, B. S. Wang, J. P. Sun, Z. L. Dun, Y. Uwatoko, G. F. Chen, X. L. Dong *et al.*, Pressure-induced superconductivity up to 9 K in the quasi-one-dimensional KMn_6Bi_5 , *Phys. Rev. Lett.* **128**, 187001 (2022).
- [14] L. Chen, L. Zhao, X. Qiu, Q. Zhang, K. Liu, Q. Lin, and G. Wang, Quasi-one-dimensional structure and possible helical antiferromagnetism of RbMn_6Bi_5 , *Inorg. Chem.* **60**, 12941 (2021).
- [15] S. Long, L. Chen, Y. Wang, Y. Zhou, S. Cai, J. Guo, Y. Zhou, K. Yang, S. Jiang, Q. Wu *et al.*, Flipping of antiferromagnetic to superconducting states in pressurized quasi-one-dimensional manganese-based compounds, *Phys. Rev. B* **106**, 214515 (2022).
- [16] E. Ising, Beitrag zur Theorie des Ferromagnetismus, *Z. Für Phys.* **31**, 253 (1925).
- [17] W. Heisenberg, Zur Theorie Des Ferromagnetismus, *Z. Für Phys.* **49**, 619 (1928).
- [18] C. S. O. Yokoi, L.-H. Tang, and W. Chou, Ground state of the one-dimensional chiral XY model in a field, *Phys. Rev. B* **37**, 2173 (1988).
- [19] N. D. Mermin and H. Wagner, Absence of ferromagnetism or antiferromagnetism in one- or two-dimensional isotropic Heisenberg models, *Phys. Rev. Lett.* **17**, 1133 (1966).
- [20] L. J. De Jongh, Experiments on simple magnetic model systems, *J. Appl. Phys.* **49**, 1305 (1978).
- [21] L. Duan, X. C. Wang, J. Zhang, Z. Hu, J. F. Zhao, Y. G. Feng, H. L. Zhang, H.-J. Lin, C. T. Chen, W. Wu *et al.*, Synthesis, structure, and magnetism in the ferromagnet La_3MnAs_5 : Well-separated spin chains coupled via itinerant electrons, *Phys. Rev. B* **106**, 184405 (2022).
- [22] L. Duan, X. Wang, F. Zhan, J. Zhang, Z. Hu, J. Zhao, W. Li, L. Cao, Z. Deng, R. Yu *et al.*, High-pressure synthesis, crystal structure and physical properties of a new Cr-based arsenide La_3CrAs_5 , *Sci. China Mater.* **63**, 1750 (2020).
- [23] J. Zhang, A. C. Komarek, M. Jin, X. Wang, Y. Jia, J. Zhao, W. Li, Z. Hu, W. Peng, X. Wang *et al.*, High-pressure synthesis, crystal structure, and properties of iron-based spin-chain compound $\text{Ba}_9\text{Fe}_3\text{Se}_{15}$, *Phys. Rev. Mater.* **5**, 054606 (2021).

- [24] L. Duan, X.-C. Wang, J. Zhang, J.-F. Zhao, L.-P. Cao, W.-M. Li, R.-Z. Yu, Z. Deng, and C.-Q. Jin, Synthesis, structure, and properties of $\text{Ba}_9\text{Co}_3\text{Se}_{15}$ with one-dimensional spin chains, *Chin. Phys. B* **29**, 036102 (2020).
- [25] L. Duan, J. Zhang, X. Wang, J. Zhao, L. Cao, W. Li, Z. Deng, R. Yu, Z. Li, and C. Jin, High-pressure synthesis, structure and properties of new ternary pnictides La_3TiX_5 ($X = \text{P}, \text{As}$), *J. Alloys Compd.* **831**, 154697 (2020).
- [26] J. Zhang, Y. Jia, X. Wang, Z. Li, L. Duan, W. Li, J. Zhao, L. Cao, G. Dai, Z. Deng *et al.*, A new quasi-one-dimensional compound Ba_3TiTe_5 and superconductivity induced by pressure, *NPG Asia Mater.* **11**, 60 (2019).
- [27] J. Zhang, M. Liu, X. Wang, K. Zhao, L. Duan, W. Li, J. Zhao, L. Cao, G. Dai, Z. Deng *et al.*, $\text{Ba}_9\text{V}_3\text{Se}_{15}$: A novel compound with spin chains, *J. Phys.: Condens. Matter* **30**, 214001 (2018).
- [28] J. Zhang, L. Duan, Z. Wang, X. Wang, J. Zhao, M. Jin, W. Li, C. Zhang, L. Cao, Z. Deng *et al.*, The synthesis of a quasi-one-dimensional iron-based telluride with antiferromagnetic chains and a spin glass state, *Inorg. Chem.* **59**, 5377 (2020).
- [29] J. Zhang, M.-L. Jin, X. Li, X.-C. Wang, J.-F. Zhao, Y. Liu, L. Duan, W.-M. Li, L.-P. Cao, B.-J. Chen *et al.*, Structure-spin-transport anomaly in quasi-one-dimensional $\text{Ba}_9\text{Fe}_3\text{Te}_{15}$ under high pressure, *Chin. Phys. Lett.* **37**, 087106 (2020).
- [30] P. F. Shan, Q. X. Dong, P. T. Yang, L. Xu, Z. Y. Liu, L. F. Shi, N. N. Wang, J. P. Sun, Y. Uwatoko, G. F. Chen *et al.*, Complex evolution of the magnetic transitions and unexpected absence of bulk superconductivity in chemically precompressed NaMn_6Bi_5 , *Phys. Rev. B* **107**, 094519 (2023).
- [31] O. Y. Zelinska and A. Mar, Ternary rare-earth manganese bismuthides: Structures and physical properties of RE_3MnBi_5 ($\text{RE} = \text{La} - \text{Nd}$) and $\text{Sm}_2\text{Mn}_3\text{Bi}_6$, *Inorg. Chem.* **47**, 297 (2008).
- [32] G. M. Sheldrick and T. R. Schneider, [16] SHELXL: High-resolution refinement, *Meth. Enzymol.* **277**, 319 (1997).
- [33] G. M. Sheldrick, A short history of SHELX, *Acta Cryst. A* **64**, 112 (2008).
- [34] See Supplemental Material at <http://link.aps.org/supplemental/10.1103/PhysRevMaterials.8.034402> for more details about the magnetic transitions of La_3MnBi_5 and discussions on the 1D magnetic susceptibility models, which includes Refs. [35–38].
- [35] G. R. Wagner and S. A. Friedberg, Linear chain antiferromagnetism in $\text{Mn}(\text{HCOO})_2 \cdot 2\text{H}_2\text{O}$, *Phys. Lett.* **9**, 11 (1964).
- [36] S. Emori, M. Inoue, M. Kishita, and M. Kubo, Magnetic properties of ammonium, sodium, and lithium pentafluoromanganates(III), *Inorg. Chem.* **8**, 1385 (1969).
- [37] H. Steinfink and I. E. Grey, Crystal structure of Ba_2MnSe_3 . Linear antiferromagnetism in Ba_2MnX_3 ($X = \text{S}, \text{Se}$), *Inorg. Chem.* **10**, 691 (1971).
- [38] A. D. J. Barnes, T. Baikie, V. Hardy, M.-B. Lepetit, A. Maignan, N. A. Young, and M. G. Francesconi, Magnetic coupling and long-range order in the spin-chain sulfide Ba_2CoS_3 , *J. Mater. Chem.* **16**, 3489 (2006).
- [39] Y. Li, Z. Jiang, J. Li, S. Xu, and W. Duan, Magnetic anisotropy of the two-dimensional ferromagnetic insulator MnBi_2Te_4 , *Phys. Rev. B* **100**, 134438 (2019).
- [40] C. Xu, J. Feng, H. Xiang, and L. Bellaiche, Interplay between Kitaev interaction and single ion anisotropy in ferromagnetic CrI_3 and CrGeTe_3 monolayers, *npj Comput. Mater.* **4**, 57 (2018).
- [41] D. Y. Yan, M. Yang, P. B. Song, Y. T. Song, C. X. Wang, C. J. Yi, and Y. G. Shi, Site mixing induced ferrimagnetism and anomalous transport properties of the Weyl semimetal candidate MnSb_2Te_4 , *Phys. Rev. B* **103**, 224412 (2021).
- [42] R. Nath, K. M. Ranjith, B. Roy, D. C. Johnston, Y. Furukawa, and A. A. Tsirlin, Magnetic transitions in the spin- $\frac{5}{2}$ frustrated magnet BiMn_2PO_6 and strong lattice softening in BiMn_2PO_6 and BiZn_2PO_6 below 200 K, *Phys. Rev. B* **90**, 024431 (2014).
- [43] J. Zhang, X. Wang, L. Zhou, G. Liu, D. T. Adroja, I. da Silva, F. Demmel, D. Khalyavin, J. Sannigrahi, H. S. Nair *et al.*, A ferrotoroidic candidate with well-separated spin chains, *Adv. Mater.* **34**, 2106728 (2022).
- [44] Y. Yafet, Ruderman-Kittel-Kasuya-Yosida range function of a one-dimensional free-electron gas, *Phys. Rev. B* **36**, 3948 (1987).
- [45] B. Willenberg, M. Schäpers, K. C. Rule, S. Süllow, M. Reehuis, H. Ryll, B. Klemke, K. Kiefer, W. Schottenhamel, B. Büchner *et al.*, Magnetic frustration in a quantum spin chain: The case of linarite $\text{PbCuSO}_4(\text{OH})_2$, *Phys. Rev. Lett.* **108**, 117202 (2012).
- [46] J. B. Yang, K. Kamaraju, W. B. Yelon, W. J. James, Q. Cai, and A. Bollero, Magnetic properties of the MnBi intermetallic compound, *Appl. Phys. Lett.* **79**, 1846 (2001).
- [47] H. Yamada and S. Takada, Magnetoresistance of antiferromagnetic metals due to s - d interaction, *J. Phys. Soc. Jpn.* **34**, 51 (1973).
- [48] K. J. Singh, S. Chaudhary, M. K. Chattopadhyay, M. A. Manekar, S. B. Roy, and P. Chaddah, First-order transition from ferromagnetism to antiferromagnetism in $\text{Ce}(\text{Fe}_{0.96}\text{Al}_{0.04})_2$: A magnetotransport study, *Phys. Rev. B* **65**, 094419 (2002).